Internship Report

May-July 2015

Study and characterization of CVD-grown single crystal graphene

Intern:
Luca Planat
Grenoble INP-Phelma

Tutor:
Dr. Stefan Heun
Senior Scientist
NEST,Insituto Nanocienze and
Scuola Normale Superiore

Acknowledgment

I would like to express my gratitude to NEST laboratory, which hosted me for 3 months and the Scuola Normale Superiore di Pisa which allowed me to live in their residential school for the same period.

I would like to thank Dr. Stefan Heun and his team: Abhishek Kumar, Yuya Murata, Stefano Guiducci and Umesh Gomes for their welcome and their kindness. I would like to give special thanks to Shaohua Xiang, who helped and taught me a lot.

Introduction

General introduction

My internship has taken place in the NEST laboratory located in Pisa, Italy. I have worked under the direction of Dr. Stefan Heun. I started to work on hybrid devices as Superconductor/ Normalconductor/Superconductor (SNS) and then on nano-devices based on graphene. I mainly worked on the graphene nano-devices thus this report will mostly focus on it.

Graphene is a one-atom thick material composed by atoms of carbon. It has remarkable electronic properties. It is generally known for being a gapless semiconductor or a semimetal. Graphene is an extraordinary and promising material and it is expected to play an important role in the future microelectronics industry. This is why it is really important to know its characteristics and thus making transport measurements on it.

There are three main ways to get graphene: mechanical exfoliation, epitaxial growth on SiC substrate, and chemical vapor deposition (CVD). The first one permits to obtain small single-crystal pieces of graphene (micrometer sized). Here, we focus on investigating the electric properties of CVD graphene.The main purpose of CVD graphene is that it is a simple and cheap way to obtain large-scale graphene for practice. One of the negative points is that it usually grows as polycrystalline graphene. Despite that, a team in the NEST laboratory was able to produce millimeter sized single-crystal graphene by CVD as we will see it later in this report. From this new way of producing CVD graphene, one of the final purposes of the graphene team of Dr. Heun is to create a narrow ribbon from this new kind of CVD graphene in order to investigate the electric properties base on Scanning Gate Microscope (SGM). During my internship, I worked on the first step of this project: characterizing this CVD graphene and making transport measurements.

As it has been said before, CVD graphene is generally known for being polycrystalline, in difference to mechanically exfoliated graphene. But CVD is a more convenient and cheaper way to obtain large-scale graphene. In order to quantify its properties, we performed low temperature transport measurements. We observed a well-known phenomenon in two dimensional electron gas (2DEG) devices (devices with a two-dimensional gas of electrons): the Weak Localization (WL) and the Weak Anti-Localization (WAL). WL is a quantum interference effect which increases the resistance of a material. Application of a magnetic field suppresses this effect. WL can therefore be detected as a peak of resistance in a small range of magnetic (e.g. between -0.05T and 0.05T), centered in B=0T. WL and WAL have already been observed in graphene since several years on exfoliated, epitaxial, and CVD graphene. The previous observations of WL & WAL on CVD graphene have been made for the great majority on polycrystalline graphene. In our case, the devices were several 10 micrometers in size.

However, the problem was to know if this new way of getting bigger flakes of CVD graphene was able to offer high-quality graphene and if it has the same characteristics with the WL as mechanically exfoliated graphene. Moreover, by analyzing the data and fitting the WL data to the theory of McCann et al., one can deduce specific scattering times and lengths of the sample such as dephasing, intervalley and intravalley scattering times/lengths.

All the experiments have been performed with lock-in technique in a Heliox Helium-3 cryostat under a perpendicular magnetic field up to 12T generated by a superconducting magnet with base temperature of 250mK. Magneto-transport measurements have been performed at several different temperatures. Two samples have been measured, called Device-A and Device-B. The dimensions are both large as 70*50 um^2. All the data have been obtained with the software LabView. Furthermore, the plots have been drawn with Origin and fitted with Mathematica.

This report is divided into two parts. The first one is a general presentation of graphene and a specific presentation of the samples. The first characterization of the devices is also presented and a brief theory of the Quantum Hall Effect in « classical » 2DEGs and in graphene is given. In the second part, we will focus on the Weak Localization, the theory and the results. Moreover, the data mining of the Weak Localization's data allows us to characterize even more the devices in order to understand better its intrinsic behavior.

Presentation of the Laboratory

The NEST laboratory (acronym for National Entreprise for nanoScience and nanoTechnology) is an interdisciplinary centre of research. The NEST laboratory has moved since several years in the old buildings of the Scuola Normale, in Piazza San Silvestro, Pisa. Since its moving in these buildings, the NEST has bigger facilities. It gathers in the same center physicists, chemists and biologists. These scientists are specialized in investigating problems at the nanoscale. The Nest houses about 150 people.

The Nest laboratory is directly affiliated to the Scuola Normale Superiore di Pisa. But the NEST intiative also comprises three other institutions: the Istituto Italiano di Tecnologia (IIT), the Consiglio Nazionale delle Ricerche (CNR) and Scuola Superiore Sant'Anna. In the physics field, the NEST laboratory is specialized in Supra/SemiConductor nanostructure design and experimental investigation. The NEST laboratory has its own Clean Room which allow researcher of the NEST to fabricate their own nano devices.

1 Presentation of the device and first characterization

1.1 Graphene

Graphene is a monolayer of graphite where atoms of carbon are packed into a honeycomb crystal [1]. It has been isolated for the first time in 2004 by Andre Geim's team at the University of Manchester. Graphene is the perfect materials to study two Dimensional electrons gas (2DEG) because it is by definition a material with only two dimensions (one atom of carbon thick). One of the main characteristics of graphene is that it is a gapless semiconductor. This means the conduction band is empty and the valence band is completely full (at T=0K), and they touch at only one point: the Dirac Point (DP). In graphene, the charge carriers are governed by Dirac's relativistic equation. It means that charge carriers act as if they were relativistic particles, with no mass and a « constant speed » at $v_F = 10^6$ m.s-1. One can tune the carrier density of graphene by applying an electric field to the graphene. Experimentally, this can be done by adding a gate above or below the piece of graphene, called topgate or backgate, respectively. By applying a voltage bias on the gate, one can tune the carrier density inside the graphene. The carrier density is zero when the backgate voltage V_{bg} is equal to a voltage corresponding to the Dirac Point, V_{dp}. Theoretically, V_{dp} is equal to zero. Because of impurities, defects, and missing atoms, the Dirac point is usually different from 0. Knowing the value of the Dirac Point is a quick way to evaluate the purity and the defect density of the samples.
There are three main ways to produce graphene:
-Mechanically exfoliated
-epitaxially grown
-CVD grown.
In this report, we will talk about the most used and « historic » one, the mechanical exfoliation, and about the CVD growth, the technique which was used to make the devices.

1.1.1 Exfoliated graphene

The first attempt to obtain graphene was by doing a mechanical exfoliation of graphite.To do so, one is supposed to put small piece of graphite on scotch tape and tear off thinner and thinner pieces of graphite. By repeating this operation several times, one can extract from it a monolayer of graphite, called graphene. This technique does not allow to obtain very big pieces of graphene (usually, one can get micrometer sized graphene). The benefits of this technique are that gives a really nice and pure piece of graphene with almost perfect crystallinity and low density of defects. This technique is still preferred for fundamental research, but it does not allow to create big graphene flakes on a large scale

1.1.2 CVD graphene

The Chemical Vapor Deposition technique consists in decomposing a carbon-containing gas on a transition metal, for example Nickel or Copper. During the process, the hydrocarbons adsorbed on the copper are very mobile and form honeycomb crystal graphene. Thanks to this way of growing graphene, one can obtain bigger flakes of graphene but in general, this kind of growing graphene does not give good crystallinity.
In this report, transport measures are performed on CVD graphene grown under a new technique reported by one of the NEST teams [2]. This new technique allows growing single-crystal CVD graphene up to a millimeter size in a quick and cheap way while maintaining a high rate of purity and a low density of defects.

1.2 Quantum Hall Effect

Our devices are made according to the model of the Hall Bar, which is a device with several electrodes: the source (where the current starts), the drain, and other electrodes on the side in order to measure longitudinal and transversal voltages. This special kind of device is most used to study the Quantum Hall Effect (QHE). We are going to see the theory of the Quantum Hall Regime

1.2.1 The Theory of the QHE

1.2.1.1 In « classical » materials [3]

Standard 2DEGs are obtained by superposition of different semiconductors differently doped. By playing on the doping, one can create a zone with a specific chemical potential where the electrons will be confined. If this zone is thin enough, one obtains a two-dimensional system, i.e. a system where the motion in one direction is quantized. Typically, the z-direction is taken as the direction quantized, while x and y directions are free. We can now build a device called Hall Bar. In this device, the electrons can only propagate in x and y. Here is a scheme of a Hall Bar:

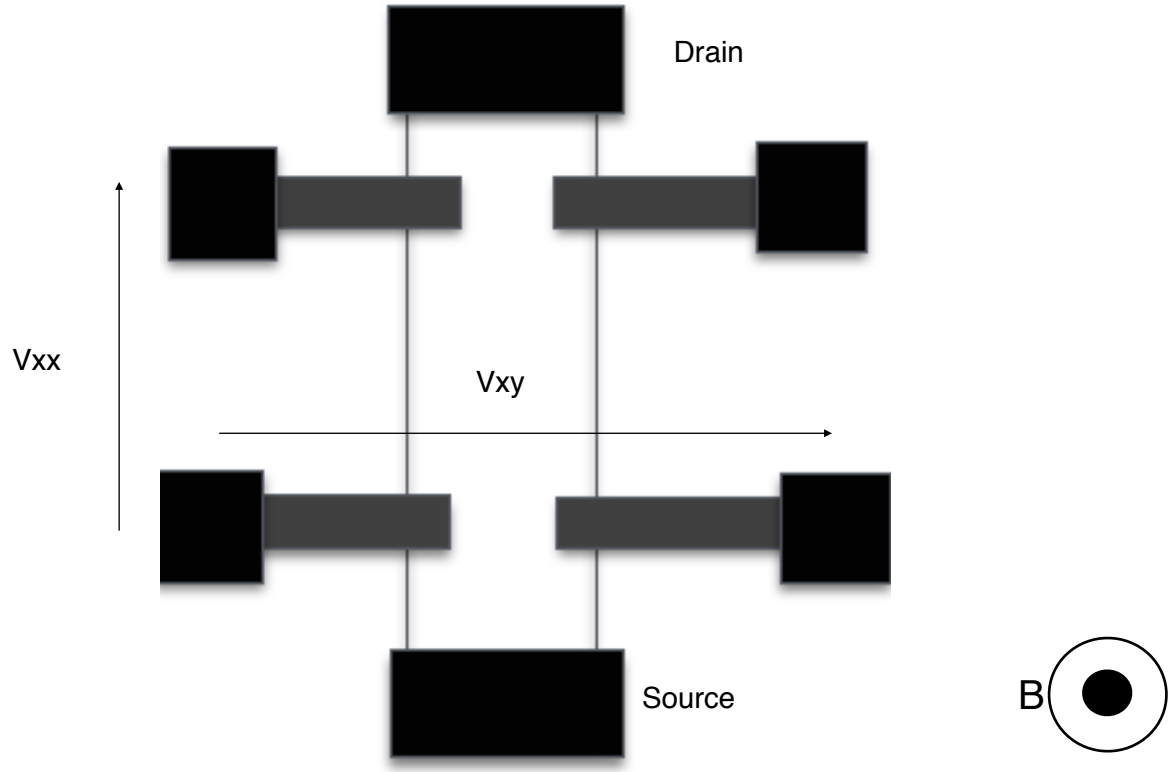

Figure 1 Scheme of a Quantum Hall Bar

One can see that a perpendicular magnetic field is applied to the device. From the classical point of view, the electron, due to Lorentz force, will be be deviated from its original path. Electrons will accumulate on one lateral sides and the charge accumulation will create an electric field and so a transversal voltage, called V_{xy}.

So far, this has been a description of the classical Hall regime based on Drude's model. The quantization in the z direction and the very low base temperature will make appear quantum phenomena. Instead of getting a linear relation between R_{xy} and B, the magnetic field, one can observe plateaus of transversal resistance. To each plateau corresponds a filling factor. At the values of B at which R_{xy} shows plateaus, the longitudinal resistance R_{xx} is 0, it means that no voltage drop is measured (the transport is dissipationless).
To determine the electron's behavior, one can use the following Hamiltonian (demonstration in appendix 1)

$$H = \frac{1}{2m}(\vec{p} + e\vec{A})^2 + V(\vec{r}) \qquad (1)$$

We find quantized energy levels (they are called Landau levels):

$$E_j = \hbar\omega(j + \frac{1}{2}) \qquad (2)$$

The degeneracy of each Landau level, i.e. the density of states of it, is:

$$n_{\text{deg}} = \frac{eB}{h} \qquad (3)$$

Let n_s be the carrier density of the material, then $\nu = n_s/n_{deg}$ is the number of filled Landau levels, hence the name « filling factor »:

$$\nu = \frac{n_s}{n_{\text{deg}}} = \frac{n_s h}{eB} \qquad (4)$$

In « classical » materials such as Si or AlGaAs and GaAs, the filling factors are always integers from 1, 2, 3, …, therefore this effect is called the integer quantum Hall effect.
In a perfect crystal, the Landau level would look like:

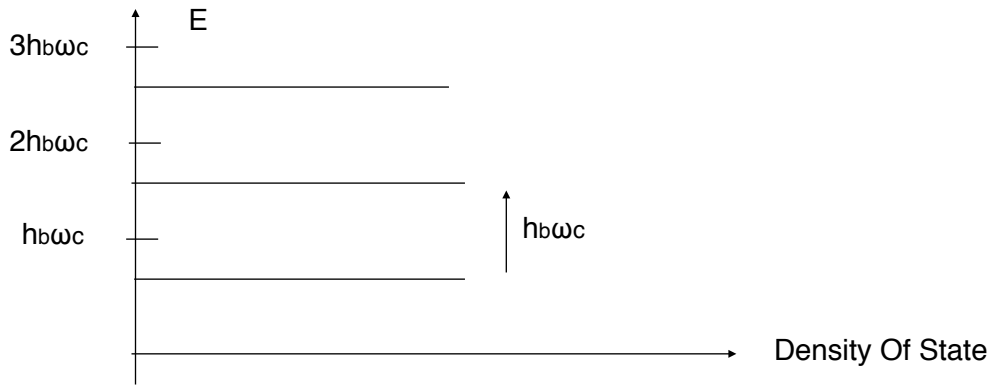

Figure 2 Landau level in a perfect crystal

In fact, due to the disorder in the 2DEG, each Landau level has a certain width. This disorder comes from the impurities inside the crystal, which create modulations of the potential. Thus, in function of the energy, the electrons will either be localized or not. If they are, no current will flow through the bulk of the device, and the conductivity S_{xx} will be equal to zero. If they are not, then S_{xx} will be different from 0. Moreover, from the charge of the electron, and the direction of the magnetic field, electrons will have always the same cyclotron motion, called chirality. Thus, only the electrons from the edge which « bounce » on the edge of the bulk will participate to the current flow

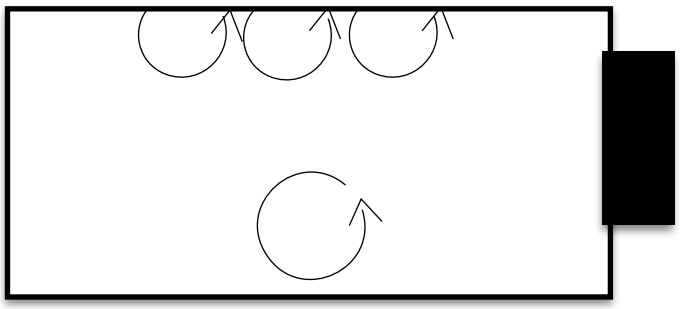

Figure 3 Electron's motion in a 2DEG

Due to their chirality, and regardless of the materials, impurities or defects in the crystal, electrons from the edge states will always follow the same path. That is why one can observe a quantization of the resistance $R=h/e^2$ which is a universal constant. The more channels are involved in the current flow (each one carrying a conductance quantum of e^2/h), the more the conductance will rise (and the resistance decrease). The higher is B , the more there are degeneracies, i.e. the more carriers can be fit into each Landau level, and therefore at a given carrier concentration, less channels used, and the more R is high. B changes n_{deg}, so it changes the filling factor v

1.2.1.2 Quantum Hall effect in graphene

In graphene, one can also observe the Quantum Hall Regime [4] because it is a 2D material where the electron gas is confined in the z direction.The quantization of the resistance and the conductance are even more spectacular because graphene is really a two-dimensional material, unlike device based on doped Silicon. The main difference comes from the filling factor. We have seen before that on standard quantum Hall effect, the filling factors are integers like 1,2,3… and so on. In graphene filling factors are 2,6,10,14,18… it comes from that in graphene, Landau levels are degenerate because charge carriers are not considered as electron but as massless Dirac Fermions, which are pseudo-particles with other properties (anomalous quantum Hall Effect). Another difference comes from that the magnetic field B is not the only parameter to sweep in order to observe plateaus. Indeed, it has been said previously that applying a voltage on a back/top gate can modify the carrier density inside the sample. Thus, one can fix a magnetic field and sweep the voltage of this gate and change the carrier density n_s. As it had been said, this will change the filling factor v. Different filling factors, corresponding to plateaus of conductivity and resistance, are reached.

1.2.2 Hall Bars

The samples which have been worked on are Hall bars shaped on CVD graphene. An example of such a device is given Fig 4. It is a graphene flake with four small electrodes and two additional ones which are bigger : the source and the drain.

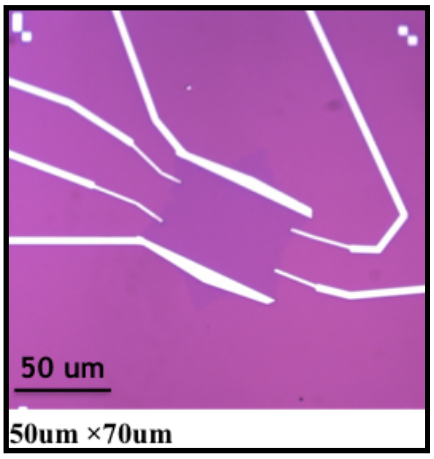

Figure 4 The device A, a Hall bar with 6 contacts

In the next part, we will see how such devices are made and how the electrical contacts and connections are fabricated in the clean room.

1.3 Preparation of the devices

All the devices are made in the Clean Room of the Nest laboratory. This part will explain the different steps required in order to obtain a Hall Bar from a sample of CVD graphene, grown at NEST.

1.3.1 In the clean room

1.3.1.1 Electron Beam Lithography (EBL)

There are different ways to fabricate electrical contacts and connections in a nanodevice. For these graphene-based nanodevices, EBL has been used. First place, one must cover the sample of CVD graphene with a solution of Polymethyl methacrylate (PMMA) which is a solution that contains extremely long chains of polymers. These chains has the property to be broken with a high-energy electron beam (up to 30KeV). Once this solution has been applied on the sample, it has to be heated up in order to harden the solution and make it solid. After that, one can use the electron beam of a scanning electron microscope (SEM) in order to exposed the desired areas (which will later become the gold-based electrical contacts).

Figure 5 EBL process

The lithography has to be very precise and must connect both the bonding pads and the graphene. To use the EBL, one must represent the chip where the graphene is in a CAD file. A CAD file is a

numerical representation of the chip. In this file the pathways are draw. The electron beam uses its own reference system, thus one must adjust the CAD file with the electron beam and the position of the chip.
Three points have to be defined between the CAD file and the chip thus they will have the same reference system. Moreover, the chip is slightly inclined because of the clamps which fix it in the SEM. Thus, for each point, the focus point of the beam has to be optimized. Once the CAD file has been calibrated with the beam the EBL can start. Once the EBL has been done, one must develop the ionized PMMA i.E. put the sample in a specific liquid that removes only the PMMA where the chains have been exposed

Figure 6 Development process

1.3.1.2 Evaporation and lift-off

Once the exposed PMMA has been removed, there is the evaporation part. This part permits to make the electrical pathways and contacts with gold. First, chrome is evaporated everywhere on the sample, then gold. For an evaporation, the pressure has to be under $3x10^{-5}$ mbar (even below: $1x10^{-5}$ mbar in our case). Then, a high-energy electron beam is directed towards the metal target of the evaporator, which heats the target, then ejects the metal atoms- chrome or gold- onto the device. The metal film grows with a speed of v=0.5 Å/s. For our devices, 10nm of chrome are put and between 70 and 75 nm of gold are put on the sample

Figure 7 Evaporation process

After that, the PMMA left over can be dissolved with Acetone: this is the lift-off process. This will also remove the metal on top of the PMMA, but not the metal in PMMA-free areas At the end, there are only chrome/gold-based electrical pathways left on the sample of graphene and on the chip.

Figure 8 Lift-off process

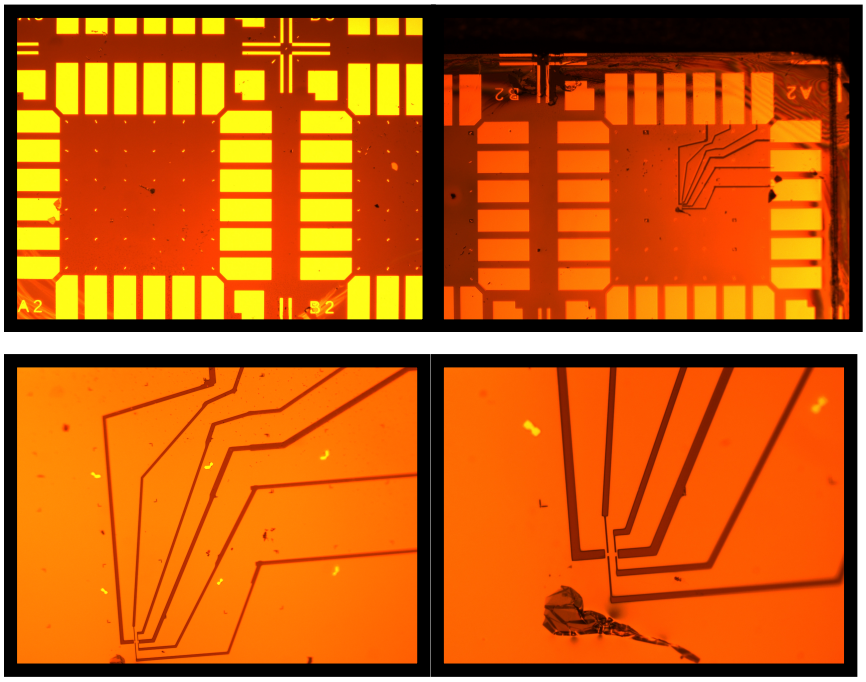

Figure 9
Pictures of the chip without graphene (left top) and pictures after the development process. The pathways start from the graphene and end on electrodes (yellow rectangles).
These parts are conductible and will be linked to chip carrier.
Bottom right: We can se the pattern of a Hall Bar device. Bigger pathways are the drain and the source

Here is the scheme of the devices A and B:

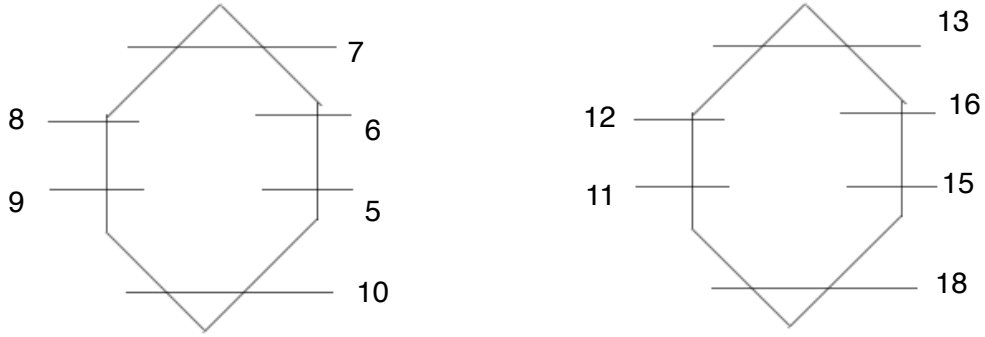

Figure 10 Scheme of the device A (left) and B

1.3.2 Bonding

After designing the Hall Bar device on the chip, this chip must be connected to a chip carrier. A chip carrier is a device which fits perfectly into a holder in the cryostat. It is convenient because there is no need to bound the device on the cryostat. The chip is fixed on the chip carrier with silver glue. Then the bonding pads of the chip (yellow rectangles in figure 9) must be connect to the bonding pads of the chip carrier. This is done thanks to a bonding tip which can res and fix a gold wire to the different pads. One must adjust the strength of the tip and the application time. After this process and the verification of all the contacts, the device is ready for experiment.

1.4 Measurements

All the transport measurements have been done in the magnet lab 0.1 of the NEST laboratory in a Heliox cryostat. All the measures have been done using the software labview.

1.4.1 Experimental conditions

All our transport measurements have been done on two CVD graphene samples [5] called device-A and device-B. Figure 4 shows Hall bar device A. One can see the single crystal gated graphene. Source and drain are the contacts 7 and 10, respectively. Measurements have been done with a constant current between source and drain $I_{sd}=10^{-7}$ Ampere. Longitudinal and transversal resistance $R_{xx}(5\text{-}6)=V_{xx}(5\text{-}6)/I_{sd}$ and $R_{xy}(6\text{-}8)=V_{xy}(6\text{-}8)/I_{sd}$, respectively, are measured in a four-point configuration. It means that two contacts are used to inject the current between source and drain (in input there is a voltage of 0.1V connect to a 1MΩ resistance (which is much larger than the resistance of the sample), therefore there is a current of 10^{-7} A flowing). The two other contacts are used to measure the voltage drop between two points (5 and 6 or 6 and 8)

All experiments are done in lock-in technique in a Heliox Helium-3 cryostat with base temperature of 250mK under a perpendicular magnetic field up to 12T generated by a superconducting magnet. Voltage was applied to a back gate (V_{bg}) to tune the carrier density of the graphene. This cryostat was a giant dewar with several tanks. The first one was filled with liquid Nitrogen at 77K and worked as a first shield. A second inner tank was filled with liquid Helium at 4.2K. A smaller tank was filled with (liquid) Helium-3 in order to get a temperature of 250mK.

1.4.2 B and Vbg

First, the objective was to observe the QHR and the different filling factors. First, the Dirac Point must be estimated in order to know at which back-gate voltage bias we obtain a zero carrier density. The value of the DP in volt is very important to characterize our devices.

The DP can be obtained by measuring the resistance between the source and the drain and sweeping the back-gate voltage. By plotting this curve, one can see a peak for a certain back-gate voltage: It corresponds to the Dirac Point.

Then, one can measure the longitudinal and transversal resistances by sweeping the magnetic field or the back-gate voltage (which corresponds to sweep the carrier density inside the graphene). The flatness of the plateaus and the observation of several plateaus can give an indication on the quality of the graphene. The best observations that we could obtain were when we swept the back-gate above and below the Dirac Point for several magnetic fields. The corresponding curves gave excellent results.

1.5 Results

1.5.1 Dirac Point

As we said previously, the first experiment to do was estimating the Dirac Point of our device.

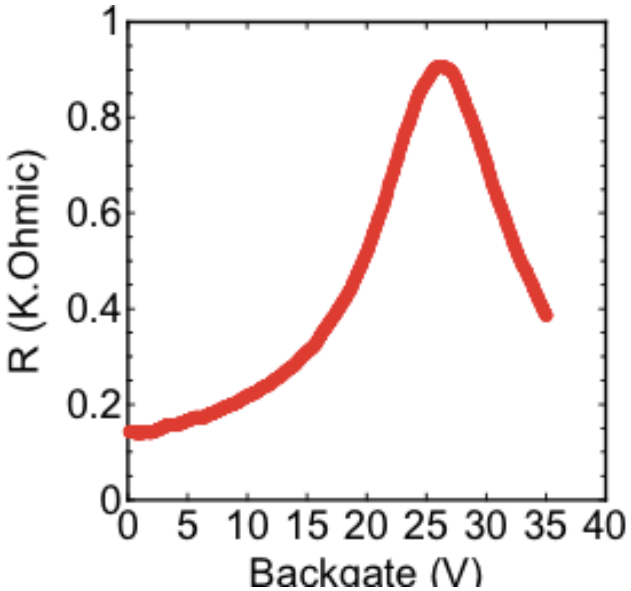

Figure 11 The resistance as a function of back gate voltage at $B = 0$T, $T = 250$mK.

The peak of resistance corresponds to a minimum of carrier density. This minimum is obtained at applied back-gate voltage V_{bg}=26V. We know now that V_{dp}=26V. This information will allow to know the link between the back-gate voltage applied and the carrier density in graphene. This link is obtained thanks to the formula [6]:

$$n = \frac{C}{e}\left|V_{DP} - V_{BG}\right| \qquad (5)$$

where e is the elementary charge (e=1,6x10^{-19} Coulomb)and C is the capacitance between the back gate and the piece of graphene (here C=11,5x10^{-9} nF.cm-2)
Thanks to this formula, the value of the carrier density at a zero back gate voltage can be calculated. The value of the DP is also a simple way to estimate the purity and quality of the graphene sample. Indeed, the closer it is to 0V, the more the sample has a low quantity of defects and contaminations. Device A has V_{dp}=26V and device B has Vdp=9V. The sample B seems to be a better sample, and this will be confirmed in the following.

1.5.2 Mobility

It measures how easy is the motion of the charge carriers inside the graphene. Mobility is measured in $cm^2/V.s$. A high value of mobility means that the crystal has a low number of impurities and missing atoms. The formula of the mobility is the following one:

$$\mu = \frac{1}{n\rho e} \qquad (6)$$

where ρ is the resistivity of the sample. Because it is a 2D material, the resistivity is calculated from the formula:

$$\rho = \frac{W}{L} R_0 \qquad (7)$$

R_0 is the resistance at zero magnetic field, W is the width of the sample, and L is the length. Naturally, R_0 depends on the value of the back gate voltage.
At 250 mK the measured mobility is 11 000 cm^2/Vs for the device B and about 9000 cm^2/Vs for the device A. These are very high values for CVD graphene.
This confirms the high quality and cleanness of these graphene samples and the superiority of the device B over the device A

1.5.3 QHE

So far, it has been shown that these samples have a very good quality. The results of the quantum Hall Effect point out once again towards same conclusion.
Here the QHE for the device B: the transversal and longitudinal resistance vs back-gate voltage.

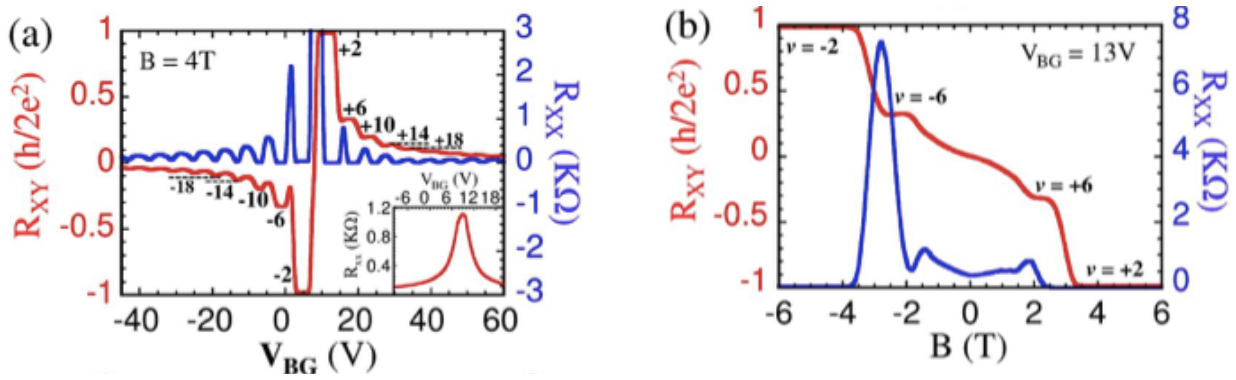

Figure 12 Rxx and Rxy vs the back gate voltage (a) and the magnetic field (b) (device B)

The figure 12 a) represents the QHR for the device B. In the inset, one can see the resistance vs V_{bg} and the peak for V_{bg} =9V. The magnetic field is 4.0T. In red is drawn the normalized (divided by h/$2e^2$, the quantum of resistance) transversal resistance. In blue is draw the longitudinal resistance. One can observe easily 12 different filling factors and conclude the good quality of this sample. The

DP can also be found with the x-value of the inflection point of R_{xy} (when it is equal to zero). At this point, the transversal resistance changes its sign: it becomes a p-type or a n-type(predominance of holes or electrons, respectively).
In the figure 12 b), one can observe the normalized transversal resistance and the longitudinal resistance but as a function of the magnetic field for $V_{bg=}$13V. One can only see two plateaus. For both of the figures, the temperatures is T=250mK

1.6 Conclusion

In this part, a general presentation of the graphene and of our samples has been made. Measurement allowed us to characterize the devices (mobility, resistivity) and quantum transport measurement, as the Quantum Hall Effect, was a very good tool to quantify the quality of our devices. The QHE can be observed either by fixing the magnetic field and sweeping back-gate voltage or fixing back-gate voltage and sweeping the magnetic field. The first option gave us very good results (12 plateaus can be observed on the figure 12.a) and indicated that our samples have good quality, better than classic CVD graphene.
In the following part, we will study another type of transport: the magnetotransport which allows us to have a better characterization of the devices A and B.

2 Weak Localization

In the previous part, we have characterized both Hall Bar devices with quantum Hall effect. It appeared that these samples have a very high quality. Here, we focus on another phenomenon linked to 2DEG devices: the Weak Localization. WL is very useful to quantified the phase coherence in graphene because the analysis of this phenomenon gives out some important information on phase coherence, such as the dephasing scattering length. We will first explain the theory of the WL, and then we will present the experiments, the results, and finally discuss them. This discussion will confirm if it is *indeed* a really good quality CVD graphene and if it could lead to a greater exploitation of this way of synthesizing graphene.

2.1 Theory of the Weak Localization

2.1.1 Physic explanation

WL and WAL are mesoscopic effects occurring in 2D conductors where quantum interferences affect low-field magnetoresistance [7]. WL is due to charge carriers' wave which are elastically scattered by defects or impurities and form closed paths. When they have the same scattering path but with opposite directions, two carriers will interfere constructively or destructively depending on their phase difference. To allow interferences, these path length must be below a certain length: the decoherence length L_f, because carriers have to keep their phase to interfere. If the interference is constructive, it will increase the backscattering process and thus the zero-field resistance. If the interference is destructive, one can see a decrease of the resistance and one can observe a dip of resistance, this is the Weak AntiLocalization (WAL). In graphene, when carriers are scattered in such path, they gain a phase difference of π because of the Berry phase [8]. Thus, one would expect that carriers would make destructive interference. But because of the elastic intervalley scattering, quantified by the intervalley scattering rate t_i^{-1}, due to the presence of atomically sharp defects and boundary effects, carriers can jump from one valley to another, breaking the chirality and making a zero phase difference between carriers. Then interference is constructive. Thus, one can observe the WL. This effect is destroyed by increasing magnetic field because it add random phase to carriers which tends to make the interference disappear by averaging it away. Thereby, when one plots the longitudinal resistance in function of B, WL is characterize by a sharp peak, theoretically centered at B=0. Inelastic phase-breaking processes can be quantified by a phase-breaking time t_f and elastic intervalley and intravalley processes by intervalley and intravalley scattering times, t_i and t_* respectively. In this figure, a scattering path of a charge carrier is shown. It has the shape of a loop:

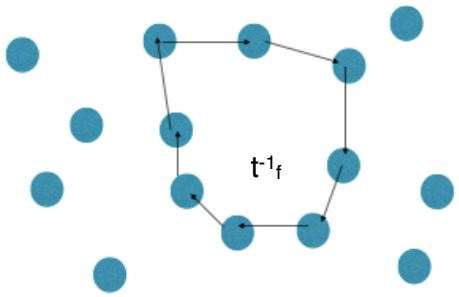

Figure 13 Scheme of scattering path

The phase-breaking rate t_f^{-1} controls the maximum size of such loops to observed an interference

phenomenon. Above this time/size, the charge carriers will have lost phase memory. In the case of the Weak Localization (and WAL), a charge carrier would have the exact same path but in the opposite direction. When two charge carriers' wave meet at a scattering spot, because of a zero phase difference, they interfere constructively, which causes a raise in the backscattering process and thus in the resistance.
WL on CVD graphene has already been studied previously. From these studies, some teams have obtained encouraging results, where experimental data fitted very well with WL in graphene theory with high mobility and dephasing lengths up to hundreds of nanometers. Previous studies which have found high mobility in CVD graphene have got dephasing lengths up to hundreds of nanometers.

2.1.2 Scattering times and lengths

As it has been said, three main scattering characterize the Weak Localization: the inelastic phase-breaking scattering (t_f), the elastic intervalley (t_i) and intravalley(t_*) scattering. The inelastic phase-breaking scatterings are mainly due to the electron-electron interaction in graphene. The lower this inelastic phase-breaking rate is, the purer the sample is. Elastic scattering rates originates from scatterers of the edge of the device ($\mathbf{t_i}$) and topological defects (t_*). Intervalley scatterings breaks the chirality and creates a zero phase difference between two charge carriers with the same scattering path.From these times/rates, one can obtain easily the scattering lengths from following a simple formula:

$$L_j = \sqrt{Dt_j} \quad (8)$$

where D is the diffusion coefficient:

$$D = \frac{1}{2} v_F l \quad (9)$$

v_F is the Fermi velocity of the charge carriers inside the graphene. Due to linear dispersion, v_F is a constant where $v_F=1.1\text{x}10^6$ m/s.
l is the mean free path. It depends on the Fermi wavenumber k_F and the resistivity ρ.

$$l = \frac{h}{2e^2 k_F \rho} \quad (10)$$

For graphene, the Fermi wavenumber is equal to:

$$k_F = \sqrt{\frac{4\pi n}{g_s g_v}} \quad (11)$$

gs and gv are respectively spin and valley degeneracies. They are both equal to 2. Thus we obtain:

$$k_F = \sqrt{\pi n} \quad (12)$$

2.2 Experimental conditions

Chronologically, the WL experiments have been performed right after the characterization and the experiments on the QHR. After the really good results found on the observation of the QHR, it has been decided to continue to investigate both of these samples. Whereas all the QHR observations have been done at a temperature of 250mK, WL experiments have been done at five different temperatures: 250mK, 1K, 4.2K, 10K, and 20K. It has been done for several temperatures in order to have the temperature dependence of this phenomenon. Moreover, we also wanted to have the back gate dependence of the WL. We measured for each temperature approximatively 10 different back-gate values, except for T=250mK where we did it for more than 20 back-gate values symmetrically above and below the Dirac Point (because it is considered as a zero carrier density). For each temperature and back-gate value, we decided to measure the magnetoresistance for B=[-0.05;0.05]T. At first it had been decided to do so for B=[-0.2;0.2]T but this turned out to be too wide to resolve the sharp WL peak.

Theoretically, on the WL results, we should have a peak centered on B=0T. Nonetheless, we observed a shift of -0.0025T when we swept the magnetic field from -0.05 to 0.05T and a shift of -0.005T when we swept the magnetic field from 0.05 to -0.05T. The origin of this phenomenon is most likely a hysteresis phenomenon coming from a residual magnetization of the environment of the device , i.e. the cryostat (even if the magnet is set to 0T, there is still a residual magnetic field which leads to a peak at a different value than 0T). To avoid this problem, we tried to set a hold time of 30 seconds between going forward and backward with the magnetic field. It did not affect the hysteresis phenomenon, confirming our initial idea of a residual magnetization. We conclude that it was not necessary to wait between going forward and backward (the main problem was to reduce the time of each measurement because there were a lot of measurements to be done). Finally, the settings for each temperature and back-gate value were:

-1001 points measurements of the resistances R_{xx} and R_{xy} for B=[+-0.05, -+0.05]T

-Each measurement lasts 100ms

-Resolution of 200uV (V_{xx} never exceeded 200uV)

-low-noise activated

-No hold time between changes of V_{bg}

With these settings, we managed to have a constant shift of -0.0020T and each measurement lasted ~100s.

2.3 Measurements

As the QHR's experiments, all the data have been acquired using LabView. To obtain the carrier density dependence, we measured the longitudinal resistance for different values of the back gate. The Dirac Point was the reference, and we took several points above it and the same number of points below it. Thus, we could see how the device would react when it is a p-type and an n-type. Because device A and B have not the same Dirac Point, we could not take the same values for the back-gate. Moreover, it has been decided to take more back-gate values for T=250mK in order to have a better knowledge of the carrier density for the very base temperature. Here is a table of all the experiments we did:

In red, we recall the value of the Dirac Point.

250mK	38	36	34.7	33.8	32.8	32.1	31.4	30.6	30	29.4	28.7	28	27.5	26.9	26	24.9	23.6	22.3	21.2	19.7	17,6	14
1K/ 4.2K/ 10K/ 20K	38		34.7		32.8		31.4				28.7				26	24.9	23.6		21.2	19.7	17.6	

Figure 14a Table of the back gate values used for the WL of the device A

250mK	18	14.3	13	11.5	10.7	10	9	8	7.75	7.25	6.9	6.5	6	5.5	4.5	3.1	0
1K/4.2K/ 10K/20K	18	14.3	13	11.5	10.7	10	9		7.75		6.9		6		4.6		0

Figure 14b Table of the back gate values used for the WL of the device B

For device A, we took 22 different back-gate values, from 38V to 14V at T=250mK. For other temperatures, only 11 values of back-gate voltage were measured. For device B, 17 values of back gate voltage have been chosen for T=250mK, and only 11 for the other temperatures.
For the WL, only the longitudinal resistance R_{xx} matters and it has been measured on the interval B=[-0.5;0.5]T. Later, in order to fit the data, we did not need $R_{xx}(B)$ but the normalized magnetoresistance $(R_{xx}(B)-R_0)/R_0^2$. That is why we needed the zero-magnetic field resistance R_0.
From the WL data $R_{xx}(B)$, R_0 was easily found because $R_0=R_{xx}(-0.0020T)$ (it was not exactly the same value for each measure, it could be from -0.0018T to -0.0023T). All the data were plotted with Origin8. From this software, we plotted first $R_{xx}(B)$ then we found R_0 then we plotted $(R_{xx}(B)-R_0)/R_0^2$. The WL data which are presented have been symmetrized. In the original data, one can see a constant slope see Fig 15. This problem has already been reported. To solve this problem, the following solution has been used: each experimental point has been replaced by (Rxx(B)+Rxx(-B))/2. In the next figure, we present an example of the symmetrized normalized magnetoresistance:

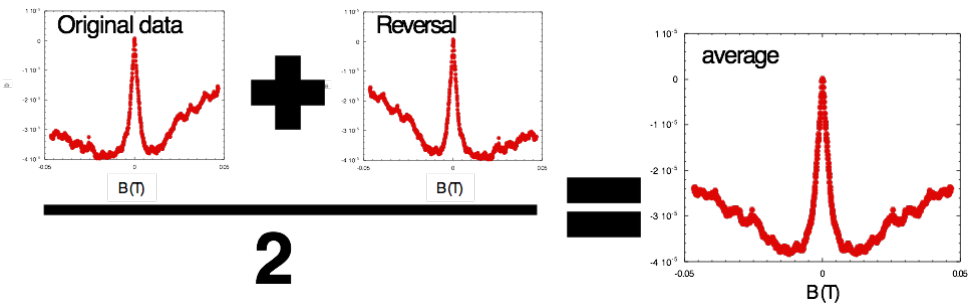

Figure 15 Symmetrization of the normalized magnetoresistance

These figures show what the magnetoresistance during the WL looks like and how the symmetrization has been made. Thanks to this method, the fitting is much more easy to do because the function used for the fitting is a symmetrical one. Furthermore, this method has been already used previously [9]. One can see that the peak is centered at zero because we added an offset of 2mT when we plotted the data.

2.4 Data Mining

2.4.1 Fitting

Once the data have been plotted in Origin8, we needed to fit them in order to get the different scattering times in order to have a better characterization of our devices. All the fits have been done using the software Mathematica. A previous post-doc (Dr. Andrea Iagallo) had already worked on the WL and send us a part of his code to fit the data. He used to work with Mathematica so it was needed to learn how this language worked. To analyze our symmetrized data, we refer to the theory of McCann et al [10]. It predicts that:

$$\frac{\Delta R_{XX}}{R_0^2} = \frac{W}{L}\frac{e^2}{\pi h}[F(\frac{\tau_B^{-1}}{\tau_\phi^{-1}}) - F(\frac{\tau_B^{-1}}{\tau_\phi^{-1}+2\tau_i^{-1}}) - 2F(\frac{\tau_B^{-1}}{\tau_\phi^{-1}+\tau_i^{-1}+\tau_*^{-1}})] \quad (13)$$

$$F(z) = \ln(z) + \Psi(\frac{1}{2}+\frac{1}{z}) \quad (14)$$

$$\tau_B^{-1} = \frac{4eDB}{\hbar} \quad (15)$$

W/L is not exactly the ratio width over length but it has to be calculated in a specific way. For the device A, this ratio is 2.63. For the device B it is 4.
Psi is the digamma function. It is the derivative of the logarithm of the gamma function. During the fitting, the three parameters to optimize were t_f, t_i, and t_*. t_f controls the width of the peak, t_i its height, and t_* its wings. We could control these parameters through the code in Mathematica. The code sent by Mr. Iagallo, enhanced and modified for our device, is put in the appendix 2

2.4.2 Parameters

In this code, the input was the carrier density, the value of R_0 and the experimental data found. Then, we had to adjust the three parameters to find the best fit of the the symmetrized experimental data. Next, we plotted all the different times as a function of the temperature and V_{bg}. From previous studies, we knew what was the general trend of the temperature and V_{bg} dependence of the scattering times. It allowed to identify points which were not aligned and verify if the WL was correctly fitted. We also knew that the phase-breaking scattering time had to be larger than the elastic scattering times (otherwise we would not have observed WL because elastic scattering must

occur much more often than inelastic scattering. If it is not the case, the phase information would be lost before the loop is completed). In the big picture, t_f was about several tens of picoseconds, ti was about several picoseconds and t* was about tenth of picoseconds, t_i was about several picoseconds, and t_* was about tenth of picoseconds. These times have specific features near the Dirac Point. It was necessary to be very careful when we approached the Dirac Point because the parameters used to change a lot. Once the parameters were correctly found, the code also gave all the points of the fit in a table. This allowed to draw the fit using another software because the Mathematica version we used was a test version and only available for 15 days

2.5 Discussion

In this part, we will discuss the results that have been found. We will discuss the temperature and carrier density dependence of the magnetoresistance and of the scattering lengths and times found by fitting the data

2.5.1 Overview of the WL

A quick overview allows us to see the temperature and carrier density of the magnetoresistance in the WL.

2.5.1.1 Carrier density dependence

In the figure 16, we show the carrier density dependence for the device A for five values: 26V, 28.7V, 30V, 32.1V and 14V (from low to high carrier density) in the magnetic field range [-0.05, 0.05]T

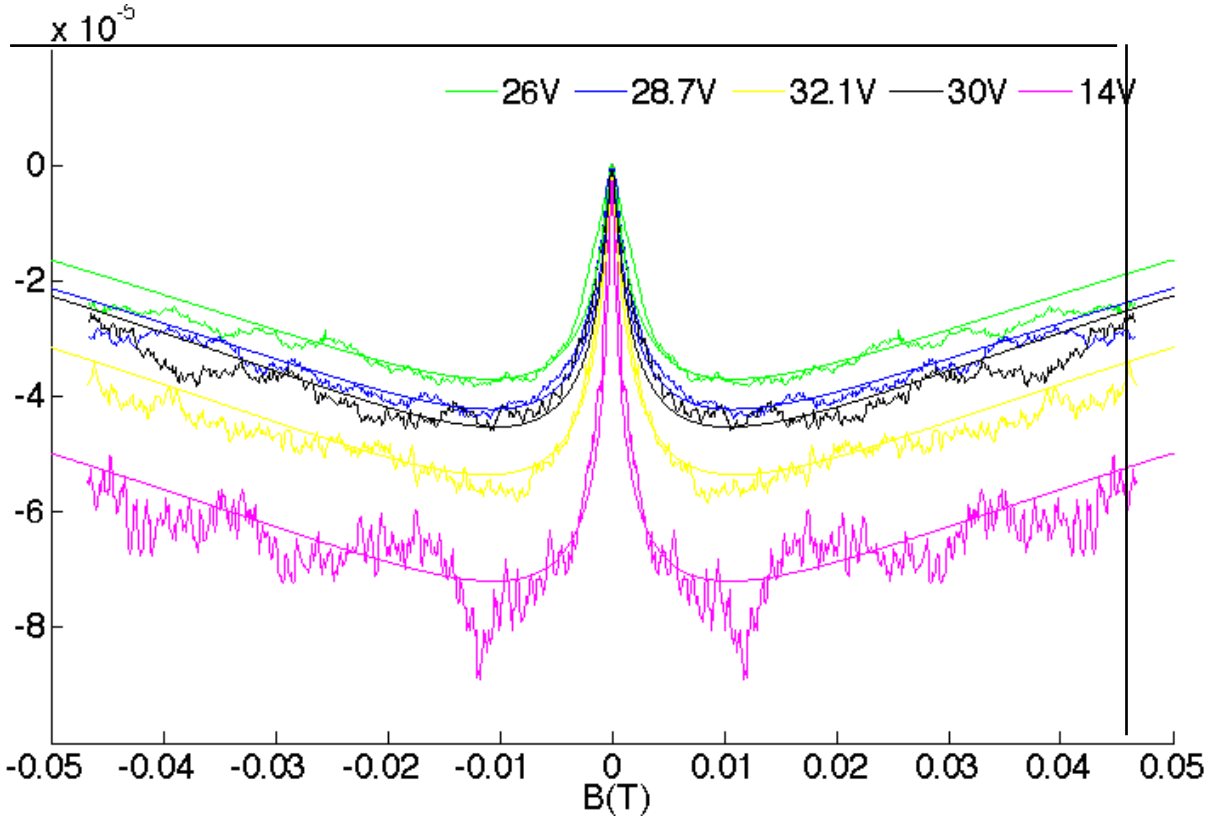

Figure 16 Normalized magnetoresistance as a function of magnetic field for five different back gate voltage for Device-A.

The first observation we can make is the difference in amplitude and width of the peak for the different carrier densities. The higher the carrier density, the more the peak will be sharp and high. One can also observe that there are more noises and oscillations after the peak when the carrier density is high. The oscillations should be the universal conductance fluctuation. A wider peak means that the phase-breaking time is small thus the charge carriers do not keep their phase for long time. The fact that the peak is also shorter means that there is a big intervalley scattering time. The fact that for low carrier density the peak is wider means that charge carriers do not have a big coherence time. We can conclude that the WL is « stronger » for high carrier density because there are more charge carriers which have the same phase and have constructive interference which creates more backscattering and rise the resistance.

2.5.1.2 temperature dependence

In this figure, one can observe the Weak Localization for several temperatures (250mK, 1K, 4.2K, 10K and 20K) in the magnetic field range [-0.05, 0.05]T

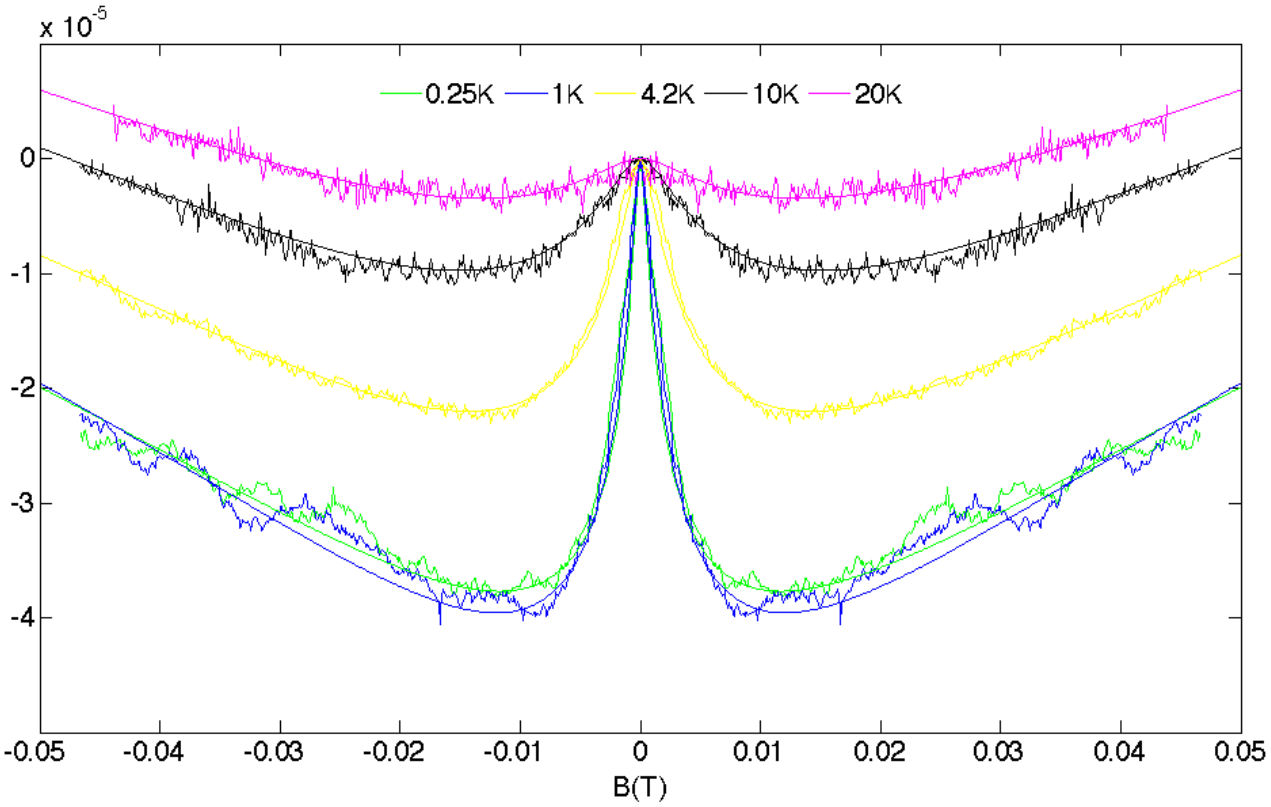

Figure 17 Normalized magnetoresistance as a function of magnetic field for five different temperature.

The first observation that one can make is the the different widths of the magnetoresistance curves in function of the temperature. The peak is wide and small for high temperatures and sharp and tall for base temperature. The WL is « stronger » for base temperature because high temperature tends to break the initial phase of the charge carriers via phonon scattering. At the base temperature, the charge carriers stay longer coherent, thus they can make more constructive interferences which increases the backscattering rates. Almost the same curve shape is observed between 0.25K and 1K. We conclude that under 1K the coherence time will be approximatively the same.

2.5.2 Scattering times

Base on our fits, we have obtained all the inelastic and elastic scattering times of the devices. Once again, it is possible to see the temperature and the carrier density of such times and for the devices A and B. Thus, it is possible to plot it and obtain a general trend of the behavior of our devices. There are several advantages to this study. First of all, we will be able to see if our CVD graphene samples follow the same trends as previous studies on graphene [11]. Second of all, it will be a way to quantify again the purity and quality of our CVD samples. If we find high values for inelastic phase-breaking times, it means that the charge carriers do not lose the initial phase. This will be a good reason to continue making studies on this CVD graphene and keep this way of synthesizing graphene. Figure 18 shows t_f, t_i, and t_* as a function of V_{bg}:

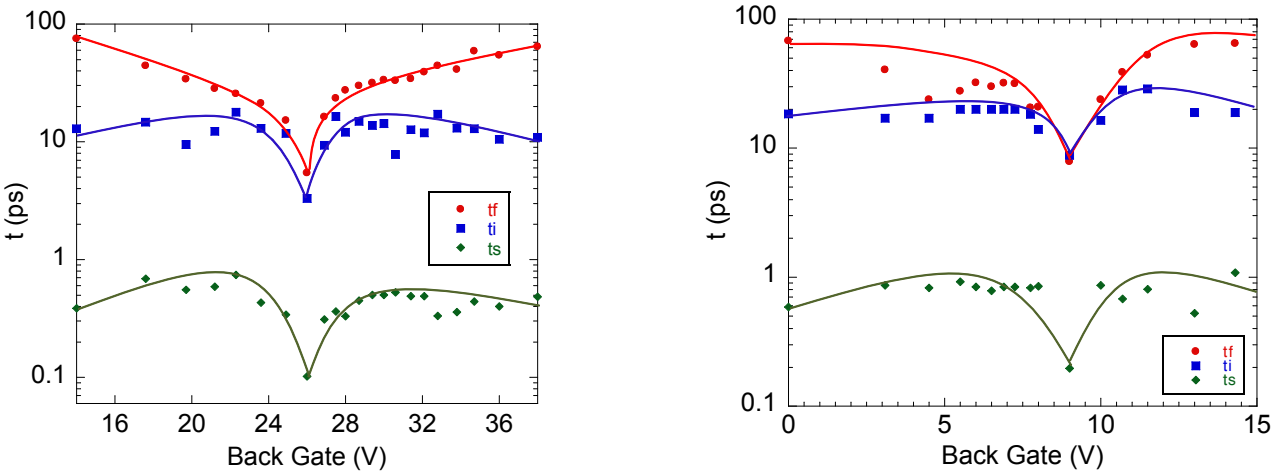

Figure 18 The scattering time as a function of back gate voltage for Device-A (left) and Device-B (right) at T = 250mK.

The general trend of these figures shows that the inelastic times are always higher than the elastic times. The intravalley scattering time is much smaller compared to the other times. Moreover, one can observe a specific trend for the inelastic time: there is a small slope before and after the Dirac Point whereas the elastic times have a constant value. However, for the three times, there is an important drop at the Dirac Point. This trend is the same for all temperatures but it is most apparent for T=250mK. When one compares with previously reported studies, one can observe that the same trends have been found for mechanically exfoliated graphene. Moreover, the times found for the inelastic scattering time are much higher for our CVD graphene sample than for those found on previous CVD graphene samples. This study of the WL tends to confirm what has been previously found during the part about the QHR: the good quality of this CVD graphene. Furthermore, the device B seems to be better than the device A.

2.5.3 Scattering Lengths

From the scattering times, one can obtain the scattering lengths by applying the formula 8. The diffusion coefficient D can be calculated providing that one has all the experimental data needed, meaning the wavenumber, the Fermi velocity and the resistivity (see equations 9 and 10). Thanks to D and the scattering times, one can obtain the plot of scattering lengths as a function of back gate voltage, as showing in figure 19.

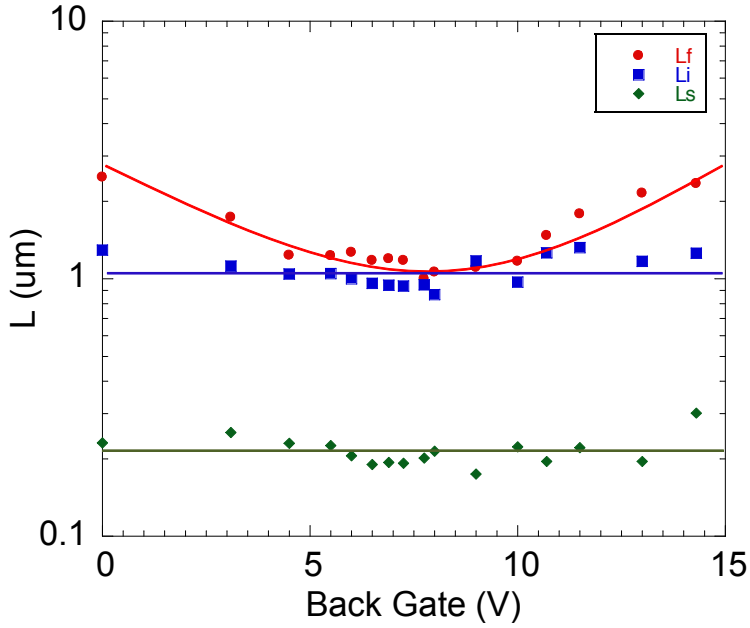

Figure 19 The scattering length as a function of back gate voltage for Device-B at $T = 250$mK.

The first observation is the absence of a carrier density dependence for the elastic scattering lengths (L_i and L_* seem to be constant). However, the dephasing length depends on the back gate voltage. One can also focus on the temperature dependence of such lengths. Figure 20 shows the temperature dependence of such lengths. In the following figure, one can see the temperature dependence of the dephasing length for 3 back-gate voltages (Dirac Point, above it, and below it) of device A.

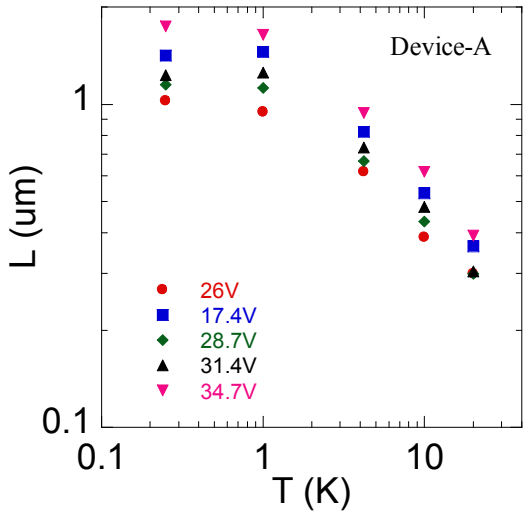

Figure 20 Scattering length as a function of temperature for five different back gate voltages for Device-A.

One can observe two different regimes: for T<1K, the dephasing length is independent of temperature. This is consistent with the previous observation in part 2.5.1.2 where the WL curves for T=250mK and for T=1K were virtually identical. For T>1K, there is a constant slope. For high temperatures, the dephasing length decreases, which is consistent with previous observations and theory: when the temperature increases, the electrons lose their phase quicker and browse a smaller path.

Finally, we can compare the dephasing lengths for both devices A and B in order to see which have the bigger length for the same carrier density.

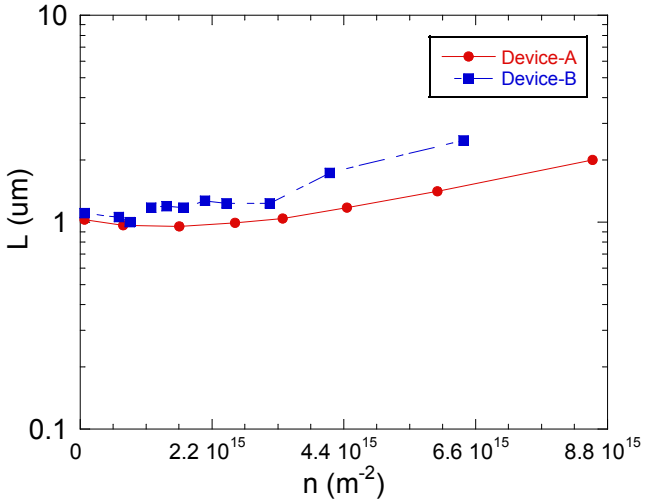

Figure 21 Dephasing length as a function of carrier density for the two device T=250mK

This figure shows that for any carrier density, the electrons of the device B have a bigger coherent path than the electrons of device A. It allows us to finally conclude on the better quality of the device B over the device A. Moreover, we find a dephasing length exceeding the micrometer. It is the same order of magnitude than for mechanically exfoliated graphene [12]. This study showed the extraordinary quality of this new kind of CVD graphene .

Conclusions

In summary, we made two different transport experiments to see if this new kind of single-crystal CVD monolayer graphene could be a good alternative to exfoliated or epitaxially grown graphene for applications. First of all, this new method appears simple and allows to get millimeter-sized single crystal graphene. Moreover, these are high purity graphene confirmed by their low Dirac Point (as small as 9V) and large mobility (up to 11000 cm^2/Vs). We observed two quantum transport phenomena: the QHE and the WL, by measuring longitudinal and transversal resistance in gated 6-contact Hall bar devices. The flatness and the regularity of the QH plateaus are the proof of the superior quality of our monolayer graphene. Furthermore the half-integer filling factor is a good indicator of the monolayer-ness of our graphene.
The study of the magnetoresistance and the Weak Localization allowed us to find characteristics of our graphene samples by fitting experimental data. Temperature and carrier density dependence (through the back gate voltage) of the inelastic and elastic scattering times have been obtained. The trends we have found are in agreements with previous work on mechanical exfoliated monolayer graphene. This process of making CVD is really attractive and allows to synthesize big-sized monolayer graphene with similar fundamental characteristics as exfoliated graphene while being more convenient to obtain.

Glossary:

2DEG: 2 Dimensional Electron Gas
BG: Back Gate
CAD:Computer-aided design
CVD: Chemical Vaporous Deposition
DP: Dirac Point
DOS: Density of State
EBL: Electron Beam Lithography
NEST: National Entrepise for nanoScience and nanoTechnology
PMMA: Polyméthacrylate methyl
QHB: Quantum Hall Bar
QHE: Quantum Hall Effect
QHR: Quantum Hall Regime
SEM:Scanning electron microscope
SGM: Scanning Gate Microscopy
WL: Weak Localization
WAL: Weak AntiLocalization

List of figures:

References

(1) A.K. Geim, K.S. Novolesov, Nature Materials 6, 183 - 191 (2007)

(2) V. Miseikis et al, 2D Mater. 2 014006 (2015)

(3)Talk-Lithuania-2011 Stefan Heun

(4)K.S Novoselov, A.K. Geim, S.V. Morozov, D. Jiang, M.I. Katnsnelson, I.V. Grigorieva, S.V. Dubonos, A.A. Firsov, Nature Lett. 438, 10 (2005)

(5) L.A Jauregui, H. Cao, W. Wu, Q. Yu, Y.P. Chen, Solid State Commun. 151 (2011) 1100-1104

(6) S. Wang, S. Suzuki, K. Furukawa, C. M. Orofeo, M. Takamura, and H. Hibino, *Appl. Phys. Lett.* **103**, 253116 (2013).

(7) F.V. Tikhonenko, D.W. Horsell, R.V. Gorbatchev, A.K. Savchenko, Phys. Review Lett. 100, 056802 (2008)

(8) T. Ando, T. Nakanishi, and R. Saito, *J. Phys. Soc. Jpn.* **67**, 2857 (1998).

(9) Iagallo, S. Tanabe, S. Roddaro, M. Takamura, H. Hibino, S. Heun, Physical Rev. B 88, 235406 (2013)

(10) E. McCann et al, Physical Review Lett, 97, 146805 (2006)

(11) H. Cao et al, Applied Phys. Lett. 96, 122106 (2010)

(12) D-K. Ki, D. Jeong, J-H Choi, H-J Lee Physical Rev. B 78, 125409 (2008)

Appendix

Appendix 1

For an electron in an external magnetic field we have the following Hamiltonian

$$H = \frac{1}{2m}(\vec{p} + e\vec{A})^2 + V(\vec{r})$$

With m the electron's mass
p the momentum of the electron
A the potential vector
And V the potential of the electron
We have a perpendicular magnetic field:

$$\vec{B} = B\vec{e}_z$$

Thus, we can choose the Landau's Gauge for the potential vector A:

$$\vec{A} = \begin{matrix} 0 \\ Bx \\ 0 \end{matrix}$$

One can verify that :

$$\overrightarrow{Rot}\vec{A} = \vec{B}$$

For the potential, we take:

$$V(\vec{r}) = 0$$

According to Schrödinger's equation:

$$H\Psi(x,y) = E\Psi(x,y)$$

which becomes:

$$\frac{1}{2m}(p_x^2 + p_y^2 + 2eBxp_y + (eBx)^2)\Psi(x,y) = E\Psi(x,y)$$

X and p_y do commute so we can write 2eBx p_y
We know that:

$$p_y\Psi(x,y) = -i\hbar(ik_y)\Psi(x,y)$$

$$p_y^2\Psi(x,y) = \hbar^2 k_y^2\Psi(x,y)$$

Thus the Schrödinger's equation becomes:

$$\frac{1}{2m}(p_x^2 + \hbar^2 k_y^2 + 2eBx\hbar k_y + (eBx)^2)\Psi(x,y) = E\Psi(x,y)$$

$$\frac{1}{2m}(p_x^2 + e^2B^2(x^2 + \frac{2x\hbar k_y}{eB} + \frac{(\hbar k_y)^2}{(eB)^2})\Psi(x,y) = E\Psi(x,y)$$

Finally, we simply by exp(iky) and with new notations:

$$(\frac{p_x^2}{2m} + \frac{1}{2}m\omega_c(x - x_0)^2\phi(x) = E\phi(x)$$

With:

$$\omega_c = \frac{eB}{m}$$

$$x_0 = -k_y l_B^2$$

$$l_B = \sqrt{\frac{\hbar}{eB}}$$

Where ω_c is the angular frequency, x_0 is the center of the cyclotron orbit and l_b is the magnetic length.
From this equation, we recognize the harmonic oscillator's equation.
Thus we know that the energy is quantified according to:

$$E_n = \hbar\omega_c(n + \frac{1}{2})$$

Appendix 2

The code on Mathematica:

```
Clear["Global`*"]
e = 1.60218*10^-19;
me = 9.10938*10^-31; h = 6.62607*10^-34; hbar = 1.05457*10^-34;
kB = 1.38065*10^-23; eo = 8.85419*10^-12; vf = 1100000;


n = 8696875000000000;
RHO = 2.63*268;

ttr = h/(2*e^2*RHO*vf*Sqrt[Pi*n]);
Dd = 0.5*ttr*vf^2;
Bf[tf_] := hbar/(4*Dd*e*tf);
Bi[ti_] := hbar/(4*Dd*e*ti);
Bs[ts_] := hbar/(4*Dd*e*ts);
F[z_] := Log[z] + PolyGamma[1/2 + 1/z];
(* tB[B_]:=4*e*Dd*B/hbar;*)

dR[B_, tf_, ti_,
   ts_] := -2.63*(e^2/(Pi*h))*(F[B/Bf[tf]] -
    F[B/(Bf[tf] + 2*Bi[ti])] - 2*F[B/(Bf[tf] + Bi[ti] + Bs[ts])]);

 SetDirectory[NotebookDirectory[]];
Init = 1; Ending = 922;
(*   Load Data: normalized magnetoresistance    *)
setN = 1;
DataImp =
  Import["/Users/lucaplanat/Desktop/D3/D3 symmetry 4.2K/D3 4.2K \
38V.txt", "Table"];
DataLength = Dimensions[DataImp[[All, 1]]][[1]]
Rxx = Table[{DataImp[[i, setN]], DataImp[[i, setN*4]] + 0.000003}, {i,
    Init, Ending, 1}];
ListLinePlot[Rxx, PlotRange -> All]


Manipulate[
 {
  Show[{ListLinePlot[Rxx, PlotRange -> All, Mesh -> All],
    Plot[dR[-B, tf, ti, ts], {B, -0.05, 0}, PlotRange -> Full],
    Plot[dR[B, tf, ti, ts], {B, 0, 0.05}, PlotRange -> Full]}],
  Timeph = tf; TimeInter = ti; TimeIntra = ts;
  }
 , {tf, 0.1*10^-15, 90*10^-12, 0.05*10^-15}, {ti, 0.01*10^-15,
  100*10^-12, 0.05*10^-15}, {ts, 0.01*10^-15, 20000*10^-16,
  0.1*10^-15}]
```

```
"ttr: " <> ToString[FortranForm[ttr]] <> " s, tau_f:" <>
 ToString[FortranForm[Timeph*10^12]] <> " s, tau_interv:" <>
 ToString[FortranForm[TimeInter*10^12]] <> " s, tau_intrav:" <>
 ToString[FortranForm[TimeIntra*10^12]] <> " s ‘’


WLFit1 = Table[{DataImp[[i, setN]],
   dR[DataImp[[i, setN]], 1.335 e - 13, 5.611 e - 14,
    1.791 e - 14 ]}, {i, 1, DataLength/2, 1}];
Export["WLFit1" <> "VTG_0V" <> "1" <> "K.txt", WLFit1, "Table"];
```

In the first paragraph, there are useful constants.
In the second paragraph, one can see the data that we had to change for each fit: the value of the carrier density, ρ which is W/L*R0.
Then we set the scattering times and the corresponding « magnetic fields » and the function F(z).
Finally, we write the fitting function dR
Then, we had to give the numbers of point of the experimental data (c.f. Ending=922). Next, we can import the data and call it R_{xx} (because setN is equals to 1, we import the column 1 and 4 (the magnetic field and the corresponding value of the transversal resistance R_{xx} (the +0.000003 corresponds to the offset we add in order to get the peak equals to zero for B=0T) under the form of a table.
Then, we use the function « manipulate » which allows to change the three parameters t_f, t_i and t_s while plotting the experimental data and the fitting function. The range of the times is given (for example from $0.1*10^{-15}$ to $90*10^{12}$ for t_f.
Finally, when the fitting is done, the different time is given under the name of tau_f, tau_interv and tau_intrav; and the all the point of the function is put in a table

Summary:
Large size and high quality single crystal CVD monolayer graphene can be grown in the NEST laboratory. By measuring the quantum Hall effect (QHE) and the weak localization (WL), we found that the characteristics of the measured CVD monolayer graphene samples are comparable to exfoliation graphene. Firstly, the mobility can even reach to 11000 cm^2/Vs at zero back-gate voltage at 0.25K. Secondly, many flat and discernible anomaly quantum Hall plateaus have been observed in all measured samples. Finally, the WL peak has been observed in a small range of magnetic field. On these samples, it has been found that the inelastic scattering lengths are larger than 1um even at charge neutral point.

Résumé:
De grands et larges cristaux de graphene de type CVD peuvent être synthétisés dans les laboratoires du NEST. En mesurant l'Effet Hall Quantique (EHQ) et la localization faible (LF), on trouve que les caractéristiques du graphene CVD monocouche sont comparables à du graphene mécaniquement exfolié. Premièrement, la mobility peut même atteindre 11000 cm^2/Vs à une tension égal à zéro pour la back-gate et à une température égal à 250mK. Deuxièmement, de nombreux plateaux, dit anormaux, plats et facilement discernables ont été observés lors de la mesure de l'Effet Hall Quantique sur les échantillons de graphene CVD. Finalement, le pic de la localization faible a été observé sur de faible échelles de champ magnétique. Avec ces échantillons, on a trouvé que les longueurs de diffusion inélastique sont supérieurs à 1 micron au point de charge neutre (le Point de Dirac)